

[18]Crown-6 rotator in spin-ladder compound of *m*-aminoanilinium([18]crown-6)[Ni(dmit)₂]^{−†}

Tomoyuki Akutagawa,^{*a} Daisuke Sato,^b Qiong Ye,^c Toru Endo,^b Shin-ichiro Noro,^{b,c} Sadamu Takeda^d and Takayoshi Nakamura^{*b,c}

Received 14th April 2010, Accepted 10th June 2010

First published as an Advance Article on the web 5th August 2010

DOI: 10.1039/c0dt00308e

Supramolecular cations of HOPD⁺([18]crown-6) and HMPD⁺([18]crown-6) were introduced into [Ni(dmit)₂][−] salts (HOPD⁺: *o*-aminoanilinium, HMPD⁺: *m*-aminoanilinium, and dmit^{2−}: 2-thioxo-1,3-dithiole-4,5-dithiolate). Alternate layers of cations and anions were observed in the two new salts of (HOPD⁺)([18]crown-6)[Ni(dmit)₂][−] (**1**) and (HMPD⁺)([18]crown-6)[Ni(dmit)₂][−] (**2**). From X-ray crystal structural analyses, solid state ¹H nuclear magnetic resonance (NMR) spectra, and dielectric constants, the thermal rotations of [18]crown-6 in both of the (HOPD⁺)([18]crown-6) and (HMPD⁺)([18]crown-6) supramolecules occurred at temperatures above ~200 K based on the orientational disorder in the crystal structures. The two-fold flip-flop motions of HOPD⁺ and HMPD⁺ cations in salts **1** and **2** were suppressed, due to the relatively large potential energy barriers. The [Ni(dmit)₂][−] anion formed π -dimer arrangements in both salts, with a layer structure by lateral sulfur–sulfur interatomic contacts. Although the simple dimer model reproduced the magnetic properties of salt **1**, the ladder arrangement of the π -dimer in salt **2** yielded the magnetic behavior of a spin-ladder with a spin-gap of 92.5 K. The temperature dependent magnetic susceptibility of salt **2** was well reproduced by the magnetic anisotropy of $J_1/J_2 \approx 8$ between the ladder-leg (J_1 : intra-dimer interaction) and ladder-rung (J_2 : inter-dimer interaction). The [18]crown-6 supramolecular rotator of (HMPD⁺)([18]crown-6) was coexistent with the spin-ladder chain of [Ni(dmit)₂][−] anions in salt **2**.

1. Introduction

Precise control of electronic structures and molecular arrangements in molecular crystals is essential to realize the desired electrical conducting and magnetic properties.^{1,2} For instance, metallic or superconducting cation radical salts have been successfully obtained by the chemical design of the well-known tetrathiafulvalene (TTF) derivative.¹ The formation of a partially occupied π -band is important to obtain highly electrical conducting molecular crystals. On the other hand, the monovalent cation radical salts of the TTF⁺ derivative can generate one $S = 1/2$ spin on the molecule, forming a variety of magnetic crystals.^{2,3} The conducting and magnetic properties in these crystals are dominated by the molecular arrangement, which is represented

by the intermolecular transfer integral (t) and intermolecular magnetic exchange energy (J).

Although the molecular arrangement in the crystals mainly determines the physical properties, the dynamic disorder with respect to the molecule arrangement sometimes plays an important role in realizing novel physical properties of molecular crystals.^{4–9} For example, the order–disorder transition of counter anion orientation in the superconducting cation radical salts of the TTF derivative affect the electrical conducting properties,⁵ and the order–disorder transition of molecular orientation yields the ferroelectric–paraelectric transition.^{6–8} Control of the dynamic properties of molecules in the crystals has the potential to achieve unique conducting, magnetic, and dielectric functions.

A large number of dynamic molecular rotators based on rotaxanes and catenanes have been developed to realize uni-directional molecular rotators in the solution phase,⁹ where the intramolecular motional freedom can be controlled by external stimuli such as thermal energy, photo-irradiation, and chemical reactions. Stepwise molecular conformational changes using isomerization processes are important design strategies to obtain rotaxane- and catenane-based uni-directional molecular rotators. On the other hand, attempts to construct solid state molecular rotators have been achieved by Garcia-Garibay for the molecular gyroscope compounds,¹⁰ where the rotator and stator units are connected through covalent bonds to maintain the crystalline rotation space. In contrast with molecular rotators in the solution phase, solid state rotators should be a key target to realize device functions and also to clarify the rotation mechanism,^{10–12} although their construction is quite difficult, due to their closest-packed crystal structures. However, the rotation frequency and symmetry have

^aPolymer Hybrid Materials Research Center, Institute of Multidisciplinary Research for Advanced Materials (IMRAS), Tohoku University, 1-1 Katahira, Aobaku, Sendai, 980-8577, Japan. E-mail: akuta@tagen.tohoku.ac.jp; Fax: +81 22 217 5655; Tel: +81 22 217 5653

^bResearch Institute for Electronic Science, Hokkaido University, Sapporo, 001-0020, Japan. E-mail: tnaka@es.hokudai.ac.jp; Fax: +81 11 706 9420; Tel: +81 11 706 9417

^cGraduate School of Environmental Science, Hokkaido University, Sapporo, 001-0020, Japan

^dFaculty of Science and Graduate School of Science, Hokkaido University, Sapporo, 060-0810, Japan

† Electronic supplementary information (ESI) available: The atomic numbering scheme, structural analysis of salts **1** and **2**, calculated structural units, ¹H NMR spectra of salt **2**, vibrational spectra, nearest-neighboring packing of the rotators in salts **1** and **2**, ESR spectra at room temperature, and DSC diagram. CCDC reference numbers 773234–773237. For ESI and crystallographic data in CIF or other electronic format see DOI: 10.1039/c0dt00308e

been recently designed in the modification of rotator or stator structures, even in the solid state.

We have been constructing supramolecular rotators of the cation-crown ether molecular assemblies in the magnetic $[\text{Ni}(\text{dmit})_2]^-$ salts (dmit^{2-} : 2-thioxo-1,3-dithiole-4,5-dithiolate).¹³ Recently, a ferroelectric–paraelectric transition was found using the molecular rotator of the (*m*-fluoroanilinium)-(dibenzo[18]crown-6) supramolecule in $[\text{Ni}(\text{dmit})_2]^-$ salt, which realized a two-fold flip-flop motion of *m*-fluoroanilinium (*m*-FAni⁺) and a dipole inversion environment in the crystal.¹⁴ In this salt, the molecular motion and dipole orientation of the *m*-FAni⁺ cation were controllable by an external electric field. When the molecular rotations can be combined with the electrical conducting, magnetic, and dielectric properties, functional solid state molecular rotator devices are expected.

Since supramolecular cation structures have structural diversity through combinations between cations (alkali metal, alkali earth metals, arylammonium *etc.*) and crown ethers, these cationic supramolecular assemblies are effective for the control of the $[\text{Ni}(\text{dmit})_2]^-$ anion arrangements and magnetic properties in the crystals. For instance, $\text{K}^+([\text{18}]\text{crown-6})$, (*meso*-1,2-diphenylethylenediammonium)([18]crown-6)₂, (anilinium)([18]crown-6) resulted in a one-dimensional antiferromagnetic Heisenberg chain, two-dimensional antiferromagnetic Heisenberg chain, and spin-ladder chain, respectively.¹³ Among this structural diversity, specific cationic assemblies between organic ammonium-crown ethers have yielded molecular rotators such as (anilinium)([18]crown-6), (adamantylammonium)(crown ethers), and (*m*-fluoroanilinium)(dibenzo[18]crown-6) in $[\text{Ni}(\text{dmit})_2]^-$ salts.¹⁵ The crystallization of these functional units occurred in a one-pot reaction by a self-assembly process through selective cation recognition by the crown ethers, and because the magnetically active $[\text{Ni}(\text{dmit})_2]^-$ anions can coexist with the supramolecular cations. The design of the anilinium cation and crown ether was essential to yield the ferroelectric crystals and rotational freedom in $[\text{Ni}(\text{dmit})_2]^-$ salts. In the ferroelectric (*m*-FAni⁺)(dibenzo[18]crown-6) $[\text{Ni}(\text{dmit})_2]^-$ salt,¹⁴ the *m*-FAni⁺ and dibenzo[18]crown-6 act as rotator and stator, respectively. When the bulky dibenzo[18]crown-6 is replaced with [18]crown-6, the rotation of [18]crown-6 could occur with the two-fold flip-flop motion of the anilinium cation, forming a dual rotation of anilinium and [18]crown-6 with different rotation symmetry and frequency.

Here, we report new supramolecular cations of *o*-aminoanilinium (HOPD^+)([18]crown-6) and *m*-aminoanilinium (HMPD^+)([18]crown-6) in $[\text{Ni}(\text{dmit})_2]^-$ salts. Two single crystals of (HOPD^+)([18]crown-6) $[\text{Ni}(\text{dmit})_2]^-$ (**1**) and (HMPD^+)([18]crown-6) $[\text{Ni}(\text{dmit})_2]^-$ (**2**) were prepared (Scheme 1), where the [18]crown-6 and HOPD^+ (and HMPD^+) cation acted as the rotator and stator, respectively. Although the rotation of both the cations was com-

pletely suppressed in the solid state, thermally induced rotation of [18]crown-6 was realized in salts **1** and **2**. Furthermore, salt **2** yielded a spin-ladder magnetic arrangement of the $[\text{Ni}(\text{dmit})_2]^-$ anion, forming a new hybrid system between the molecular rotator and the spin-ladder magnetic property.

2. Results and discussion

2.1 Cation conformations

Cation exchange reactions from (*n*-Bu₄N⁺)[$\text{Ni}(\text{dmit})_2]^-$ to HOPD⁺ and HMPD⁺ in the presence of [18]crown-6 yielded monovalent $[\text{Ni}(\text{dmit})_2]^-$ salts of (HOPD^+)([18]crown-6) $[\text{Ni}(\text{dmit})_2]^-$ (**1**) and (HMPD^+)([18]crown-6) $[\text{Ni}(\text{dmit})_2]^-$ (**2**). In both salts, the 1:1 adducts of supramolecular cations between the organic cation and [18]crown-6 were constructed by six N–H⁺ ⋯ O hydrogen-bonding interactions, forming a stand-up configuration of the C–N bond of the anilinium unit with respect to the mean oxygen plane of [18]crown-6 (Fig. 1). The angles between the C–N bond and the mean oxygen plane of [18]crown-6 in salts **1** and **2** were 84.5 and 88.0°, respectively. The steric repulsion between the *o*-amino group of HOPD⁺ and [18]crown-6 induced slight deviation from the right angle of the C–N bond with respect to the mean oxygen plane of [18]crown-6.

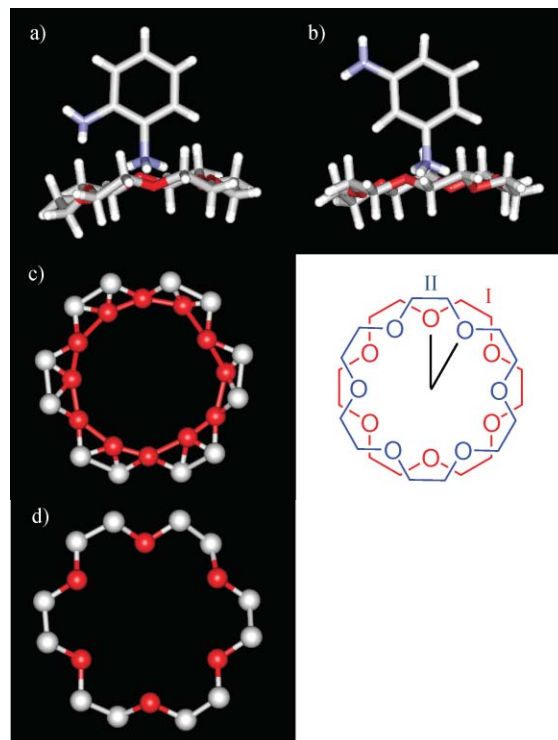
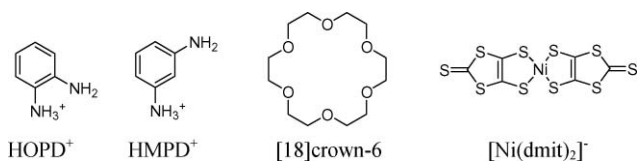


Fig. 1 Supramolecular cation structures of a) (HOPD^+)([18]crown-6) in salt **1** and b) (HMPD^+)([18]crown-6) in salt **2**, viewed normal to the π -plane of the aminophenyl ring. c) Orientational disorder of [18]crown-6 in salt **1** at temperatures above 300 K. Two [18]crown-6 orientations (**I** and **II**) were overlapped with each other (right). d) Structure of [18]crown-6 in salts **1** and **2** at 150 K.

Fig. 1a and b show the (HOPD^+)([18]crown-6) and (HMPD^+)([18]crown-6) structures viewed along the mean oxygen plane of [18]crown-6. Each (HOPD^+)([18]crown-6) and



Scheme 1 Molecular structures of *o*-aminoanilinium (HOPD^+), *m*-aminoanilinium (HMPD^+), [18]crown-6, and $[\text{Ni}(\text{dmit})_2]^-$.

(HMPD⁺)([18]crown-6) structural unit was crystallographically independent in salts **1** and **2**. Average hydrogen-bonding N...O distances between the ammonium nitrogen and oxygen atoms of salts **1** and **2** were 2.97 and 2.94 Å, respectively, which were comparable to the standard N-H...O hydrogen-bond length.¹⁶ In salt **1**, a weak N-H...O hydrogen-bonding interaction between the *o*-amino group of the HOPD⁺ cation and the oxygen atom of [18]crown-6 was observed in the N-O distance of 3.013(3) Å, whereas interatomic contacts within the (HMPD⁺)([18]crown-6) unit were not observed in salt **2**.

Orientalional disorder of the *o*- and *m*-amino groups in the HOPD⁺ and HMPD⁺ cations was not observed by structural analyses at 300 K, which suggests that the two-fold flip-flop motions of *o*-aminophenyl and *m*-aminophenyl groups were suppressed in the crystals, which was consistent with the potential energy calculations. On the other hand, orientational disorder of [18]crown-6 was observed in the crystal structural analysis of salt **1** at temperatures above 300 K. The second [18]crown-6 orientation-II began to appear at 300 K (Fig. 1d), in which the twelve carbon atoms were shared by the first orientation-I and the second orientation-II. The oxygen atoms of orientation-II appeared at the 30° rotated phase of the first orientation-I. The occupancy factor of orientation-II at 300 K was approximately 0.1, which suggests that orientation-I was a major component at 300 K with respect to orientation-II. The occupancy factor of orientation-II increased with increase in the temperature from 0.90:0.10 at 300 K, 0.80:0.20 at 330 K, to 0.75:0.25 at 360 K.

Thermally activated rotation of [18]crown-6 in salt **1** resembled that in Cs⁺₂([18]crown-6)₃[Ni(dmit)₂]₂ salt (**3**),^{15a} which also exhibited two [18]crown-6 orientations at 300 K. Although the orientational disorder of [18]crown-6 was not observed in salt **2**, the [18]crown-6 rotation was confirmed from temperature dependent solid state ¹H NMR measurements (see Solid state ¹H NMR). The average thermal parameters of the six oxygen atoms of [18]crown-6 at 300 K (*B*_{eq} = 6.16) in salt **2** were two times larger than those at 150 K (*B*_{eq} = 3.31), which suggests the thermal motions of [18]crown-6 around 300 K. The differences in disorder from the X-ray crystal structural analyses corresponded to the different shapes of the hindering potential for rotation of [18]crown-6 in salts **1** and **2**.

2.2 Packing structures of cations and [Ni(dmit)₂]⁻ anions

Each [Ni(dmit)₂]⁻ anion had one *S* = 1/2 spin, and the arrangement of [Ni(dmit)₂]⁻ anions directly determined the magnetism. Transfer integrals based on extended Hückel molecular orbital calculations were used to evaluate the magnitude of the intermolecular interactions between [Ni(dmit)₂]⁻ anions within the crystals.¹⁷ The magnetic exchange energy (*J*) is proportional to the square of the transfer integral, $J \approx 4t^2/U_{\text{eff}}$, where *U*_{eff} is the effective on-site Coulomb repulsive energy in the solid.¹⁸ Table 1 summarizes the transfer integrals (*T* = 300 and 150 K) and magnetic parameters of salts **1** and **2**.

Alternate layer structures of cations and anions were observed in salts **1** and **2**. Fig. 2a shows the unit cell of salt **1** viewed along the *a*-axis. The [Ni(dmit)₂]⁻ anionic and (HOPD⁺)([18]crown-6) cationic layers within the *ab*-plane were elongated along the *c*-axis. Each (HOPD⁺)([18]crown-6) cation was arranged at antiparallel configurations along the *b*-axis (Fig. 2b), forming face-to-face

Table 1 Transfer integrals (*t*) and magnetic parameters of salts **1** and **2**

	1		2	
<i>T</i> /K	300	150	300	150
<i>t</i> ₁ /meV ^a	89.7	92.7	-52.6	-64.3
<i>t</i> ₂ /meV ^a	-18.9	-20.0	18.3	20.0
<i>t</i> ₃ /meV ^a	-8.87	-0.23	5.17	5.38
<i>d</i> _{dimer} /Å	3.69	3.63	3.62	3.59
[Ni(dmit) ₂] ⁻ arrangement	Dimer		Two-leg ladder	
<i>g</i> (298 K) ^b	2.0522		2.0402	
Δ <i>v</i> (298 K)/mT ^b	15.9		12.24	
<i>C</i> /emu K mol ⁻¹	0.398		0.371	
θ or <i>J</i> / <i>k</i> _B /K	-82.6		<i>J</i> ₁ = -102	<i>J</i> ₂ = -10.2
Magnetism ^c	S-T		S-L	

^a The transfer integrals (*t*) were obtained from the LUMO of [Ni(dmit)₂]⁻ based on the extended Hückel calculation (*t* = -10*S* eV, where *S* is the overlap integral) at 150 K. ^b The *g*-value (*g*) and line-width (Δ*v*) of the [Ni(dmit)₂]⁻ anion were determined from the electron spin resonance spectra for single crystals at 298 K. ^c S-T and S-L are the singlet-triplet thermal excitation and spin-ladder models, respectively.

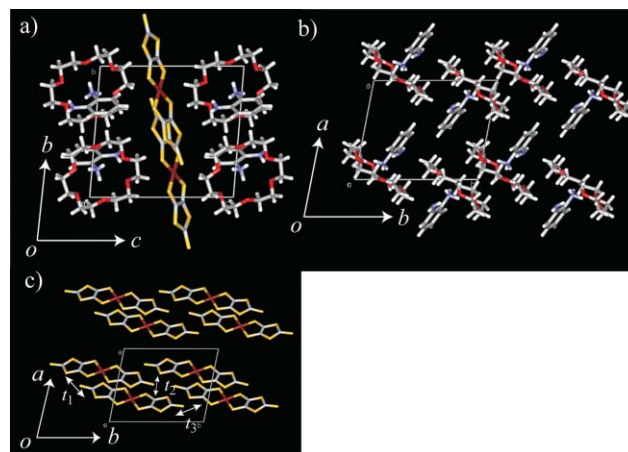


Fig. 2 Crystal structures of salt **1**. a) Unit cell viewed along the *a*-axis. b) (HOPD⁺)([18]crown-6) cation arrangement within the *ab*-plane viewed along the *c*-axis. c) [Ni(dmit)₂]⁻ anion arrangement within the *ab*-plane. Three types of intermolecular interactions (*t*₁-*t*₃) were observed.

dimers of [18]crown-6 molecules. Around the *o*-aminophenyl ring, two nearest-neighboring [18]crown-6 molecules presented steric hindrance, which restricted the two-fold flip-flop motion of the *o*-aminophenyl group within HOPD⁺ cation. Fig. 2c shows the [Ni(dmit)₂]⁻ anion arrangements within the *ab*-plane. Three types of intermolecular interactions of *t*₁ = 92.7, *t*₂ = -20.0, and *t*₃ = -0.23 meV (*T* = 150 K) were observed with magnitudes of *t*₁ > *t*₂ ≫ *t*₃ (Table 1). Among these, the π-stacking interaction between the [Ni(dmit)₂]⁻ anions (*t*₁) was the most effective interaction to determine the magnetic exchange energy (see Magnetic susceptibility).

The cation and anion packing in salt **2** was different from that in salt **1**. Fig. 3a shows the unit cell of salt **2** viewed along the *a*-axis, where the alternate cationic and anionic layers were elongated along the *b*-axis. The (HMPD⁺)([18]crown-6) supramolecular cations are stacked along the *a*-axis, which is the same cation arrangement of the spin-ladder compound of (anilinium)([18]crown-6)[Ni(dmit)₂]⁻ (**4**).¹³ⁱ Although the two-fold rotation of anilinium in salt **4** has been confirmed, the orientation of the HMPD⁺ cation in

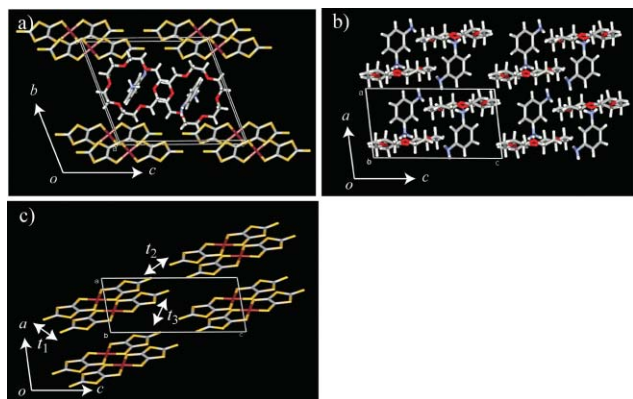


Fig. 3 Crystal structures of salt **2**. a) Unit cell viewed along the a -axis. b) (HMPD⁺)([18]crown-6) cation arrangement within the ac -plane viewed along the b -axis. c) [Ni(dmit)₂]⁻ anion arrangement within the ac -plane. Three types of intermolecular interactions (t_1 – t_3) were observed.

salt **2** was fixed without the orientational disorder of the m -amino group (Fig. 3b). In addition, the dual rotation of anilinium and [18]crown-6 in salt **4** was confirmed in the (anilinium)([18]crown-6) cation arrangement in the ac -plane. However, the large steric hindrance between the m -amino group of the HMPD⁺ cation and two nearest-neighbor [18]crown-6 molecules in the ac -plane completely suppressed the two-fold flip-flop motion of the HMPD⁺ cation. Therefore, the pinwheel rotation of [18]crown-6 in the fixed HMPD⁺ cation and [Ni(dmit)₂]⁻ anion configuration occurred in the crystal.

The [Ni(dmit)₂]⁻ anion arrangement in salt **2** is the same as that of salt **4**, resulting in a two-leg spin ladder arrangement of [Ni(dmit)₂]⁻ anions. The [Ni(dmit)₂]⁻ π -dimer with the intermolecular interaction of $t_1 = -52.6$ meV ($T = 300$ K) is connected through the lateral sulfur–sulfur interaction of $t_2 = 18.3$ meV along the long-axis of the anions. Two equivalent t_2 -interactions connect each [Ni(dmit)₂]⁻ π -dimer along the $a+c$ -axis, forming the two-leg ladder [Ni(dmit)₂]⁻ anion arrangement. The directions of the t_1 - and t_2 -interactions correspond to the ladder-leg and ladder-rung interactions, respectively. The small magnitude of the inter-ladder t_3 -interaction (5.17 meV) along the a -axis can be ignored. When the t_1 -interaction is much larger than the t_2 -interaction, the magnetic behavior should be governed by the simple dimer model. In contrast, the comparable magnitudes of the t_1 - and t_2 -interactions manifest in the spin-ladder magnetic behavior. The $t_1 : t_2$ ratio of approximately 3 : 1 at 300 K formed the magnetic interactions between the ladder-leg direction (J_1) and the ladder-rung (J_2) of the $J_1 : J_2 \approx 9 : 1$ at 300 K. Spin-ladder behavior has been reported in the $J_1 : J_2 \approx 8 : 1$ of salt **4**;¹³ⁱ therefore, similar magnetic behavior was expected in salt **2** (see Magnetic susceptibility).

2.3 Solid state ¹H NMR

On the basis of the temperature dependent crystal structures, the orientational disorder of [18]crown-6 in salt **1** occurred at 300 K due to the appearance of the second [18]crown-6 orientation. The temperature-dependent solid state wide-line ¹H NMR spectra of salts **1** and **2** were evaluated to provide evidence of the thermally induced [18]crown-6 rotations.

Fig. 4a shows the temperature-dependent spectral changes of salt **1**. The line-width ($\Delta\nu$) shows a clear broadening by

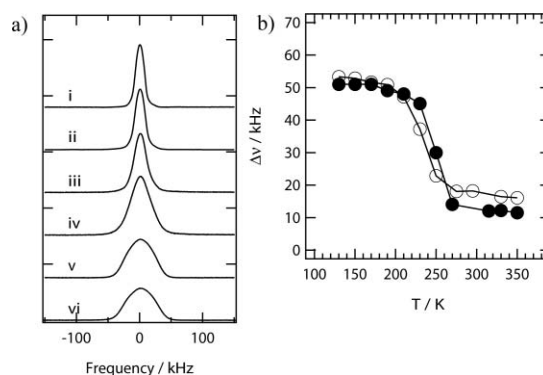


Fig. 4 Temperature-dependent solid state wide-line ¹H-NMR spectra of salts **1** and **2**. a) Spectral changes of salt **1** by decreasing the temperature from i) 350, ii) 295, iii) 250, iv) 230, v) 190, to vi) 130 K. b) Temperature-dependent maximum slope width ($\Delta\nu$) of salts **1** (○) and **2** (●).

lowering of the temperatures from 350 K (spectrum i) to 130 K (spectrum vi). The (HOPD⁺)([18]crown-6) cation in salt **1** has thirty-three protons in total (24 aliphatic protons of [18]crown-6, 4 aromatic protons of HOPD⁺, and 5 amino and ammonium protons of HOPD⁺). Since the number of [18]crown-6 protons is approximately three times greater than those of the others, the changes in the $\Delta\nu$ values are mainly governed by the motion of the [18]crown-6 molecule of salt **1**. The $\Delta\nu$ narrowing at high temperatures corresponds to the thermally induced motional (rotational) narrowing arising from [18]crown-6. The $\Delta\nu$ of 16 kHz at 350 K was about three times smaller than that of 53 kHz at 130 K. Although the orientational disorder of [18]crown-6 was not observed in the X-ray crystal structural analysis of salt **2**, almost the same temperature dependent $\Delta\nu$ changes were observed in the ¹H NMR spectra (see Fig. S4†).

Fig. 4b shows the temperature dependent $\Delta\nu$ of salts **1** and **2**. A rapid decrease in the $\Delta\nu$ values from ca. 55 to ca. 15 kHz at around 230 K was observed in salt **1**, whereas that from ca. 55 to ca. 12 kHz occurred at almost the same temperature in salt **2**. The $\Delta\nu$ – T plots of salts **1** and **2** indicate the rotational frequency of the [18]crown-6 molecules increased up to a few tens of kHz at ca. 200 K, although the orientational disorder of [18]crown-6 was not observed in salt **2**. The difference in the X-ray crystal structures of salts **1** and **2** at 300 K indicates the difference in shape hindering potential for rotation.

2.4 Potential energy of phenyl rotation within a cation

The rotation modes of supramolecular cations in the solid state were determined from the potential energy curve and the magnitude of the potential energy barrier (ΔE). The potential energy curves for the molecular rotation of aminophenyl groups within cations in salts **1** and **2** were calculated using the RHF/6-31(d) basis set.¹⁹ Since the energy changes for the rotation of NH₃⁺ group with the fixed configuration of o -aminophenyl and m -aminophenyl groups was quite significantly small in magnitude (< 5 kJ mol⁻¹), the rigid rotations of o -aminophenyl and m -aminophenyl groups around the C–N bond with the fixed configuration of –NH₃ group were evaluated. Besides the supramolecular cation, the nearest-neighbor molecules of [18]crown-6 or [Ni(dmit)₂]⁻ were included in the calculations (Fig. 5a and b).

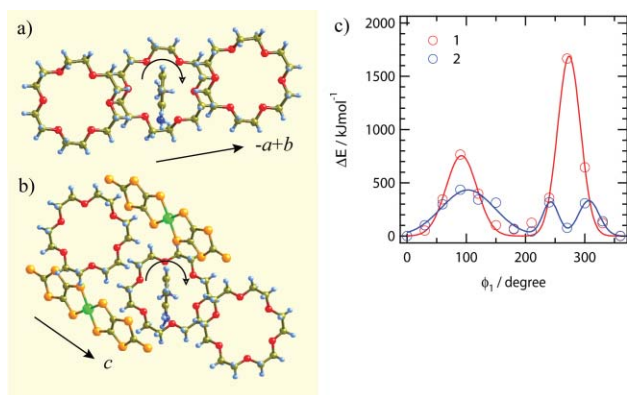


Fig. 5 Potential energy curves for the two-fold flip-flop motion of *o*-aminophenyl and *m*-aminophenyl group in salts **1** and **2**, respectively. Calculated structures of a) (HOPD⁺)([18]crown-6)₃ in salt **1** and b) (HMPD⁺)([18]crown-6)₃[Ni(dmit)₂]₂ in salt **2**. c) Potential energy (ΔE) vs. rotation angle ϕ_1 plots for salts **1** (red) and **2** (blue) around the C–N bond. The blue and red lines show line fitting to the data.

The structures of (HOPD⁺)([18]crown-6)₃ and (HMPD⁺)([18]crown-6)₃[Ni(dmit)₂]₂ were firstly evaluated for calculations of the two-fold flip-flop motions (Fig. 5a and b). In the rotational angle (ϕ_1) dependence of the relative energy (ΔE) in salts **1** and **2**, the relative energy at $\phi_1 = 0^\circ$ corresponds to the atomic coordinate from the X-ray crystal structural analysis and is defined as zero (Fig. 5c). In both salts, two nearest-neighboring [18]crown-6 molecules largely affected and restricted the two-fold flip-flop motion. The steric hindrance of the *o*-aminophenyl ring from the two nearest-neighboring [18]crown-6 molecules in salt **1** was larger than that in salt **2**.

Aside from the first potential energy minimum at $\phi_1 = 0^\circ$, the second potential energy minimum was observed around $\phi_1 = 180^\circ$. The C–N bond was inclined approximately 5° with respect to the mean oxygen plane of [18]crown-6, so that an asymmetric double-minimum potential energy curve with energy barriers of 800 and 1700 kJ mol⁻¹ was observed for salt **1**. Assuming the relaxation process of the HOPD⁺ cationic arrangement for each ϕ_1 angle, the average potential energy barrier of ca. 1200 kJ mol⁻¹ would represent the energy barrier for the two-fold flip-flop motion of the *o*-aminophenyl group in salt **1**. The large energy barrier for salt **1** completely suppressed the two-fold flip-flop motion, which is consistent with the X-ray crystal structural analysis.

The potential energy curve for the two-fold flip-flop motion of the *m*-aminophenyl group in salt **2** is affected by the two nearest-neighboring [18]crown-6 and two [Ni(dmit)₂]⁻ anions (Fig. 5b). The π -plane of HMPD⁺ cations in salt **2** are arranged at an angle of 45° with respect to the *c*-axis, so that the two [Ni(dmit)₂]⁻ anions affect the potential energy profile. The first and second energy minima were observed at $\phi_1 = 0^\circ$ and 180° with a potential energy barrier of ca. 500 kJ mol⁻¹, whereas the third energy minimum was observed at $\phi_1 = 270^\circ$ with an energy barrier of 400 kJ mol⁻¹. The interaction between the HMPD⁺ cation and the two nearest-neighboring [Ni(dmit)₂]⁻ anions yielded an asymmetric triple-minimum potential energy curve. However, the two-fold flip-flop motion of the *m*-aminophenyl group was suppressed due to a relatively large energy barrier of ca. 500 kJ mol⁻¹, which was one order of magnitude larger than that of salt **4** (40 kJ mol⁻¹). Although the structural relaxation around

the rotators will decrease the potential energy barrier in contrast with the rigid rotations, the flip-flop motions of *o*-aminophenyl and *m*-aminophenyl groups should be restricted due to the quite large potential energy barriers.

The ¹H NMR measurements of salts **1** and **2** suggest [18]crown-6 rotations at temperatures above 200 K. In the temperature dependent crystal structural analysis of salt **1**, the second [18]crown-6 orientation-**II** appeared at temperatures above 300 K, where the occupancy factors of orientation-**I** and -**II** were 0.9 and 0.1, respectively. When the rotation environments of orientation-**I** and -**II** are same as each other, almost equivalent occupancy factors are expected in the crystal structural analysis at 300 K. An idealized C_{3v} molecular symmetry of [18]crown-6 would result in alternate oxygen atoms at the upper and lower positions to the mean oxygen plane of [18]crown-6, so that equivalent oxygen sites in the C_{3v} symmetry would appear at every 120° rotation of [18]crown-6.²⁰ The idealized C_{3v} symmetry of the [18]crown-6 in salt **2** corresponds to a three-fold rotation symmetry, whereas the appearance of orientation-**II** in salt **1** suggested a twelve-fold rotation symmetry (Fig. 1).

The intermolecular interactions between the cation and [18]crown-6 in salts **1** and **2** were different. The hydrogen-bonding interaction between the *o*-amino group of the HOPD⁺ cation and oxygen atoms of [18]crown-6 was observed by a N–O distance of 3.013(3) Å in the (HOPD⁺)([18]crown-6) of salt **1** (Fig. S7[†]), whereas the hydrogen-bonding interaction between the *m*-amino group of the HMPD⁺ cation and [18]crown-6 was observed at an N–O distance of 3.0162(16) Å along the stacking direction of the (HMPD⁺)([18]crown-6) cations (Fig. S7[†]). From this perspective, the rotation environments of [18]crown-6 in salts **1** and **2** were different.

2.5 Dielectric properties

Temperature-dependent dielectric constants (ϵ_1) of salts **1** and **2** were examined to evaluate the molecular motions of supramolecular cations.²¹ Fig. 6a and b show plots of the frequency dependence ϵ_1 – T for single crystals **1** and **2** measured along the *c*- and *b*+*c*-axes, the directions of which are normal to the molecular axis of the HOPD⁺ and HMPD⁺ cations. From the crystal structural analyses and ¹H NMR measurements, the thermally activated rotations of [18]crown-6 or the thermal fluctuations of the HOPD⁺ and HMPD⁺ cations along the C–N axis could contribute to

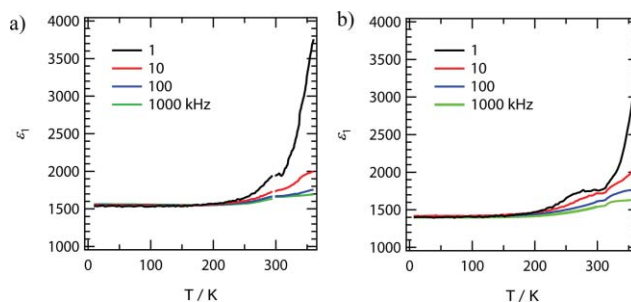


Fig. 6 Temperature- and frequency-dependent dielectric constants (ϵ_1) of salts a) **1** and b) **2**. The dielectric constants of salts **1** and **2** were measured along the *c*- and *b*+*c*-axes, respectively, the directions of which were perpendicular to the rotation axis of the HOPD⁺ and HMPD⁺ cations, respectively.

the temperature- and frequency-dependent dielectric behavior. Because the rotation of [18]crown-6 resulted in a very small magnitude dipole moment change, the dielectric response should also be of small magnitude.

In both salts, the frequency- and temperature-dependent ϵ_1 were observed at temperatures above *ca.* 200 K at low-frequency (*ca.* 1 kHz). Relatively slow molecular motion in the crystals can be assigned to the thermal rotation of [18]crown-6 and/or thermal fluctuations of the HOPD⁺ or HMPD⁺ cations. ¹H NMR measurements indicate that the frequency of rotation of the [18]crown-6 in salts **1** and **2** increased up to a few tens of kHz at *ca.* 200 K, which is almost consistent with the appearance of the frequency-dependent ϵ_1 responses at temperatures above 200 K. Broad frequency-dependent ϵ_1 maxima of salts **1** and **2** were observed at around 300 and 270 K, respectively, with increasing temperature.

When the frequency of the molecular motions coincides with the measurement frequency, a dielectric peak should appear in the ϵ_1 - T plots. The typical rotation frequency of [18]crown-6 in the Cs⁺₂([18]crown-6)₃[Ni(dmit)₂]^{-15a} and (anilinium⁺)([18]crown-6)[Ni(dmit)₂]^{-15d} salts around 230 K was estimated to be \sim 10 kHz from the solid state ¹H NMR spectra. Since the weak ϵ_1 maxima around *ca.* 300 K in salts **1** and **2** were inconsistent with the rotation frequency of \sim 10 kHz at 230 K, the thermal fluctuation of HOPD⁺ and HMPD⁺ cations contributed to the dielectric responses. On the other hand, relatively large ϵ_1 responses at the temperatures above 300 K were observed at the low-frequency measurements. Such a large ϵ_1 response was not observed in the molecular motion of the nonpolar molecule. Therefore, the thermal motion of the polar molecule contributes to the large dielectric responses at high temperature.

The two-fold flip-flop motions of the *o*-aminophenyl and *m*-aminophenyl groups were suppressed from the large potential energy barriers. The thermal fluctuation of the polar cations, *i.e.*, the pendulum motion of the HOPD⁺ and HMPD⁺ cations, resulted in the large ϵ_1 responses. The thermal molecular motion of supramolecular cations should be frozen at temperatures below 200 K, which results in the temperature independent ϵ_1 behavior. The ϵ_1 values of salts **1** and **2** at temperatures below 200 K (ϵ_1 *ca.* 1500) are dominated by the polarized π -electron on the [Ni(dmit)₂]⁻ anion. The anisotropic π -electron distribution on the [Ni(dmit)₂]⁻ anions causes the anisotropic dielectric behavior (Fig. S8–S12[†]), where large ϵ_1 values are observed in the measurement along the long-axis of the [Ni(dmit)₂]⁻ anion.

2.6 Magnetic properties

The temperature dependent molar magnetic susceptibility (χ_{mol}) per [Ni(dmit)₂]⁻ anion was directly affected by the anion arrangements in the crystals. Fig. 7a shows a plot of χ_{mol} vs. T for salt **1**. The strong π -dimerization of [Ni(dmit)₂]⁻ anions in salt **1** results in the singlet–triplet thermal excitation behavior of the two $S = 1/2$ spins.²² χ_{mol} has a broad maximum at around 100 K that tends toward zero at lower temperatures. The behavior corresponds well to the singlet–triplet dimer model (blue line in Fig. 7a) with a Curie constant (C) of 0.398 emu K mol⁻¹ and a magnetic exchange energy (J) of -82.6 K. The singlet spin state between the π -dimer is the essential intermolecular interaction in salt **1**, which is consistent

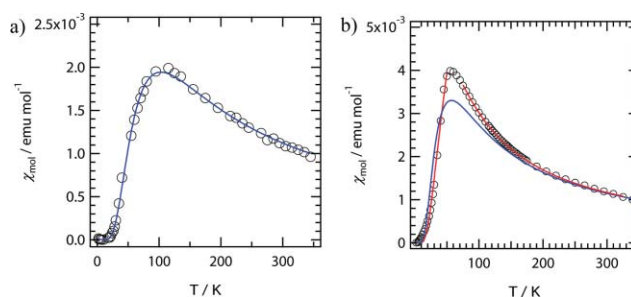


Fig. 7 Temperature dependent magnetic susceptibility of a) salt **1** and b) salt **2**. The blue and red lines represent the line fits obtained using the singlet–triplet thermal excitation model and the spin-ladder model, respectively.

with the large intra-dimer t_1 interaction (*ca.* 90 meV) in the transfer integral.

Although the overall $\chi_{\text{mol}}-T$ behavior of salt **2** almost resembles that of salt **1**, the magnetic interaction between [Ni(dmit)₂]⁻ anions in salt **2** does not follow the simple dimer model (blue line in Fig. 7b). In the crystal structure, the formation of a spin-ladder arrangement of [Ni(dmit)₂]⁻ anions was confirmed by the magnitude of the ladder-leg ($t_1 = -52.6$ meV) and ladder-rung interactions ($t_2 = 18.3$ meV). The almost zero magnitude χ_{mol} value at 2 K was rapidly increased with increasing temperature, and exhibited a broad maximum at *ca.* 50 K. The spin-ladder model reproduces the magnetic behavior of the isomorphous (anilinium)([18]crown-6)[Ni(dmit)₂]⁻ salt (**4**) well; therefore, we applied the same spin-ladder model to the $\chi_{\text{mol}}-T$ behavior of salt **2** (red line in Fig. 7b). Firstly, a low temperature limit eqn (1) was applied to the spin-ladder model,²³

$$\chi_{\text{mol}} = \alpha T^{-1/2} \exp(-\Delta/T) \quad (1)$$

where α is the constant used to determine the spin-gap (Δ). The low temperature $\chi_{\text{mol}}-T$ behavior of salt **2** was well reproduced by eqn (1) using $\Delta = 92.5$ K (low temperature red line in Fig. 7b). The magnetic exchange energies along the ladder-leg (J_1) and ladder-rung (J_2) directions could be estimated from the Δ value, assuming a ratio of the squares of the transfer integrals ($J \approx t^2$). A ratio of $t_1^2/t_2^2 \approx 10$ ($T = 150$ K) was applied for the J_1/J_2 ratio, which resulted in $J_1 = 102$ K and $J_2 = 10.2$ K based on $\Delta = 92.5$ K using eqn (2),

$$\Delta = |J_1| - |J_2| + 1/2(|J_2|^2/|J_1|) \quad (2)$$

On the other hand, the high temperature $\chi_{\text{mol}}-T$ behavior was reproduced by the high-temperature limit eqn (3),

$$\chi_{\text{mol}} = C[T^{-1} - 1/2(|J_2| + 1/2|J_2|)T^{-2} + 3/16|J_1J_2|T^{-3}] \quad (3)$$

The $\chi_{\text{mol}}-T$ behavior at high temperature was well fitted using $J_1 = 92.5$ and $J_2 = 13.6$ K (Fig. 7b) with $C = 0.371$ emu K mol⁻¹. The $J_1/J_2 \approx 7$ from the high temperature limit eqn (3) was almost consistent with $J_1/J_2 \approx 8.3$ from the squares of the transfer integrals at 300 K. The magnetic behavior of salt **2** followed the spin-ladder model, where the three-fold [18]crown-6 rotation coexists with the spin-ladder arrangements of [Ni(dmit)₂]⁻ anions.

3. Conclusions

Hydrogen-bonding assemblies between HOPD⁺ and/or HMPD⁺ and [18]crown-6 formed supramolecular cations of (HOPD⁺)([18]crown-6) and (HMPD⁺)([18]crown-6) in [Ni(dmit)₂]⁻ salts. Alternate layers of cations and anions were observed in the (HOPD⁺)([18]crown-6)[Ni(dmit)₂]⁻ (**1**) and (HMPD⁺)([18]crown-6)[Ni(dmit)₂]⁻ (**2**) salts. The large potential energy barriers for the two-fold flip-flop motion along the C–NH₃⁺ bond of the HOPD⁺ and HMPD⁺ cations fixed the cation orientation in the crystals. On the other hand, thermally induced [18]crown-6 rotations were confirmed in both salts at temperatures above 200 K, as evidenced from temperature dependent solid state ¹H NMR and dielectric constant measurements. The thermally induced [18]crown-6 rotation was observed in the ¹H NMR measurements at *ca.* 200 K with the frequency dependent dielectric response (*T* > 200 K), whereas the thermal fluctuations of the HOPD⁺ and HMPD⁺ cations contributed to the large dielectric responses at temperatures above 300 K. The magnetic properties of salt **1** were dominated by the strong π -dimerization of [Ni(dmit)₂]⁻ anions, which followed the singlet–triplet dimer model with the magnetic exchange energy of *J* = –82.6 K. The [Ni(dmit)₂]⁻ π -dimers were connected as two-leg ladder arrangements, where the ratio of the ladder-leg and ladder-rung interactions was approximately 8:1 at 150 K, based on the squares of the transfer integrals. The temperature dependent magnetic susceptibility of salt **2** was well explained by the spin-ladder model in both the low- and high-temperature regions. The magnetic exchange energies for the ladder-leg and ladder-rung directions were 92.5 and 13.6 K, respectively, using the low temperature limit equation. A spin-ladder chain of [Ni(dmit)₂]⁻ anions coexists in the supramolecular rotator of [18]crown-6 in salt **2**. The coupling between the magnetism and molecular rotators should be an important target to realize novel phase transition systems.

4. Experimental

4.1 Synthesis of (*o*-aminoanilinium⁺)(BF₄⁻) and (*m*-aminoanilinium⁺)(BF₄⁻)

42% HBF₄ aq. solution (9.8 mmol) was slowly added dropwise into a solution of *o*-aminoaniline or *m*-aminoaniline (10 mmol) in CH₃CN (30 mL) over a period of 10 min. The solvent was removed under reduced pressure and a white powder was recrystallized from CH₂Cl₂–hexane. Elemental analyses. (HOPD⁺)(BF₄⁻); Calcd. for C₆H₉N₂BF₄; C: 36.78, H: 4.63, N: 14.30. Found. C: 36.03, H: 4.87, N: 13.93. (HMPD⁺)(BF₄⁻); Calcd. for C₆H₉N₂BF₄; C: 36.78, H: 4.63, N: 14.30. Found. C: 36.77, H: 4.62, N: 14.34%.

4.2 Preparation of salts **1** and **2**

The monovalent precursor (*n*-Bu₄N)[Ni(dmit)₂] salt was prepared according to the literature.²⁴ Single crystals of salts **1** and **2** were obtained by the standard diffusion method in an H-shaped cell (*ca.* 50 mL). A green solution of (*n*-Bu₄N)[Ni(dmit)₂] (40 mg) in CH₃CN (*ca.* 20 mL) was poured into a solution of (HOPD⁺)(BF₄⁻) or (HMPD⁺)(BF₄⁻) (*ca.* 100 mg) in the presence of [18]crown-6 (*ca.* 400 mg) in CH₃CN (*ca.* 30 mL) (detailed conditions for single crystal preparation are shown in Table S1†). After two weeks, single crystals (typical dimensions: 0.4 × 0.2 × 0.1 mm) were obtained as black plates. The stoichiometry of the crystals was determined by X-ray structural and elemental analyses. Elemental analyses. Salt **1**: Calcd. for C₂₄H₃₃N₂O₆S₁₀Ni; C: 34.95, H: 4.03, N: 3.40. Found. C: 34.95, H: 3.97, N: 3.22. Salt **2**: Calcd. for C₂₄H₃₃N₂O₆S₁₀Ni; C: 34.95, H: 4.03, N: 3.40. Found. C: 34.45, H: 3.99, N: 3.50%.

4.3 Crystal structure determination

Crystallographic data (Table 2) were collected using a Rigaku RAXIS-RAPID diffractometer with Mo-K α (λ = 0.71073 Å)

Table 2 Crystal data, data collection, and reduction parameter of salts **1** and **2**

	1 (150 K)	1 (300 K)	2 (150 K)	2 (300 K)
Chemical formula	C ₂₄ H ₃₃ N ₂ O ₆ S ₁₀ Ni	C ₂₄ H ₃₃ N ₂ O ₆ S ₁₀ Ni	C ₂₄ H ₃₃ N ₂ O ₆ S ₁₀ Ni	C ₂₄ H ₃₃ N ₂ O ₆ S ₁₀ Ni
Formula weight	824.83	824.83	824.83	824.83
Space group	<i>P</i> $\bar{1}$ (#2)	<i>P</i> $\bar{1}$ (#2)	<i>P</i> $\bar{1}$ (#2)	<i>P</i> $\bar{1}$ (#2)
<i>a</i> /Å	10.6094(4)	10.780(5)	8.2754(6)	8.334(4)
<i>b</i> /Å	12.5348(7)	12.576(7)	14.0310(10)	14.025(6)
<i>c</i> /Å	13.6440(7)	13.666(7)	16.2836(10)	16.325(9)
α /deg	82.4953(19)	82.92(2)	110.176 (2)	109.876(20)
β /deg	75.4226(14)	75.67(2)	95.932(2)	95.93(2)
γ /deg	77.7356(18)	78.02(2)	91.287(2)	90.928(18)
<i>V</i> /Å ³	1710.27(14)	1750.9(15)	1761.8(2)	1782.2(15)
<i>Z</i>	2	2	2	2
<i>T</i> /K	150(1)	300(1)	150(1)	300(1)
<i>D</i> _{calc} /g cm ⁻³	1.602	1.564	1.555	1.537
μ /cm ⁻¹	12.18	11.902	11.828	11.693
Reflections measured	16663	16994	16921	17208
Independent reflections	7707	7873	7960	7994
Reflections used	6858	5805	6809	6196
<i>R</i> _{int}	0.021	0.038	0.020	0.018
<i>R</i> ^a	0.028	0.0510	0.0361	0.0326
<i>R</i> _w (<i>F</i> ²) ^a	0.042	0.0883	0.0424	0.0430
GOF	0.903	0.400	1.111	1.145

^a $R = \sum \|F_o\| - |F_c| / \sum \|F_o\|$ and $R_w = (\sum \omega(|F_o| - |F_c|)^2 / \sum \omega F_o^2)^{1/2}$.

radiation from a graphite monochromator. Structural refinements were made using the full-matrix least-squares method on F^2 . Calculations were performed using the Crystal Structure and SHELX97 software packages.²⁵ Parameters were refined using anisotropic temperature factors except for the hydrogen atom and disordered oxygen atoms of [18]crown-6 in salt **1** at 300 K. CCDC numbers: 773234–773237.†

4.4 Calculations

The calculations for potential energy curves of the two-fold flip-flop motion of *o*-aminophenyl and *m*-aminophenyl groups were evaluated to determine the possible molecular motions in the crystals. The relative energies of the structures were calculated using the RHF/6-31(d) basis set.¹⁹ The nearest-neighboring molecules around the HOPD⁺ and HMPD⁺ cations were included in the calculations of the potential energy curves. The structural units of salts **1** and **2** for the calculations of two-fold flip-flop motions were (HOPD⁺)([18]crown-6)₃ and (HMPD⁺)([18]crown-6)₃[Ni(dmit)₂]₂, respectively (see Fig. S5 and S6†). The atomic coordinates of salts **1** and **2** obtained from the X-ray crystal structural analysis were used for the calculations. The rigid rotations of *o*-aminophenyl and *m*-aminophenyl groups around the C–N bond with the fixed NH₃⁺ configuration were evaluated in salts **1** and **2**. Since the potential energies of the *o*-aminophenyl and *m*-aminophenyl groups rotation were largely affected by the steric repulsion between the *o*- and *m*-amino groups of the cation and [18]crown-6, the rotation angles of the *o*- and *m*-amino groups were structurally optimized. The transfer integrals (t) between the [Ni(dmit)₂][−] anions were calculated within the tight-binding approximation using the extended Hückel molecular orbital method. The LUMO of the [Ni(dmit)₂][−] molecule was used as the basis function.¹⁷ Semi-empirical parameters for Slater-type atomic orbitals were obtained from the literature.¹⁷ The t values between each pair of molecules were assumed to be proportional to the overlap integral (S) via the equation $t = -10S$ eV.

4.5 Dielectric measurements

Temperature-dependent dielectric constants were measured by the two-probe AC impedance method at a frequency of 100 kHz (HP4194A) with a single crystal placed in a cryogenic refrigeration system (Daikin PS24SS). Electrical contacts were prepared using gold paste (Tokuriki 8560) to attach the 10 μm φ gold wires to the single crystal. The measurement axes of salts **1** and **2** were perpendicular to the molecular axis of [18]crown-6 with the HOPD⁺ and HMPD⁺ cations.

4.6 Solid state ¹H NMR measurements

Solid-state wide-line ¹H nuclear magnetic resonance (NMR) spectra under static sample conditions were measured by solid echo pulse sequence $\pi/2_x - \tau - \pi/2$, ($\pi/2$ pulse width and τ were 1.3 and 10 μs, respectively) using a Bruker DSX 300 spectrometer with an operating frequency of 300 MHz for protons.

4.7 Magnetic susceptibility

The temperature-dependent magnetic susceptibility and the magnetization-magnetic field dependence were measured with

a Quantum Design MPMS-XL5 SQUID magnetometer using polycrystalline samples. The applied magnetic field was 1 T for all temperature dependent measurements.

Acknowledgements

This work was partly supported by a Grant-in-Aid for Science Research from the Ministry of Education, Culture, Sports, Science, and Technology of Japan.

Notes and references

- (a) J. M. Williams, J. R. Ferraro, R. J. Thorn, K. D. Carlson, U. Geiser, H. H. Wang, A. M. Kini and M.-H. Whangbo, *Organic Superconductors*, Prentice-Hall, New Jersey, 1992; (b) T. Ishiguro, K. Yamaji and G. Saito, *Organic Superconductors*, P. Fulde ed., Springer-Verlag, New York, 1998; (c) J. Fraxedas, *Molecular Organic Materials*, Cambridge University Press, Cambridge, 2006.
- (a) J. S. Muller and A. J. Epstein, *Angew. Chem., Int. Ed. Engl.*, 1994, **33**, 385; (b) O. Kahn, *Molecular Magnetism*, VCH, NY, 1993; (c) *Magnetism: Molecules to Materials*, J. S. Miller and M. Drillon ed., Wiley-VCH, Weinheim, 2001.
- See for example (a) T. Enoki and A. Miyazaki, *Chem. Rev.*, 2004, **104**, 5449; (b) L. Ouahab and T. Enoki, *Eur. J. Inorg. Chem.*, 2004, 933.
- (a) *The Plastically Crystalline State*, J. N. Sherwood ed., John Wiley & Sons, Chichester, 1979; (b) W. C. Hamilton and J. A. Ibers, *Hydrogen Bonding in Solid*, W. A. Benjamin Inc., NY, 1968; (c) N. G. Parsonage and L. A. K. Staveley, *Disorder in Crystals*, Oxford University Press, Oxford, 1978.
- (a) M. A. Beno, G. S. Blackman, P. C. W. Leung and J. M. Williams, *Solid State Commun.*, 1983, **48**, 99; (b) C. P. Heidmann, H. Schwenk, K. Andres and F. Wudl, *Z. Phys. B: Condens. Matter*, 1984, **58**, 7; (c) V. Ilakovac, S. Ravy, K. Boubekeur, C. Lenoir, P. Batail and J. P. Pouget, *Phys. Rev. B: Condens. Matter*, 1997, **56**, 13878.
- (a) M. E. Lines and A. M. Glass, *Principles and Applications of Ferroelectric and Related Materials*, Clarendon Press, Oxford, 1977; (b) F. Jona and G. Shirane, *Ferroelectric Crystals*, Dover Publications Inc, NY, 1993.
- (a) A. Katrusiak and M. Szafranski, *Phys. Rev. Lett.*, 1999, **82**, 576; (b) T. Akutagawa, S. Takeda, T. Hasegawa and T. Nakamura, *J. Am. Chem. Soc.*, 2004, **126**, 291.
- (a) J. Fujioka, S. Horiuchi, F. Kagawa and Y. Tokura, *Phys. Rev. Lett.*, 2009, **102**, 197601; (b) P. Jain, N. S. Dalal, B. H. Toby, H. W. Kroto and A. K. Cheetham, *J. Am. Chem. Soc.*, 2008, **130**, 10450; (c) S. Horiuchi and Y. Tokura, *Nat. Mater.*, 2008, **7**, 357; (d) S. Horiuchi, R. Kumai and Y. Tokura, *Chem. Commun.*, 2007, 2321.
- (a) *Molecular Switches*, B. L. Feringa, ed., Wiley-VCH, Weinheim, 2001; *Molecular Machines and Motors*, J.-P. Sauvage ed., Springer, Berlin, 2001; (b) *Molecular Devices and Machines*, V. Balzani, M. Venturi, and A. Dredi, ed., Wiley-VCH, Weinheim, 2003; (c) *Molecular Machines Special Issue in Acc. Chem. Res.* 2001, **34**, 412; (d) V. Balzani, V. Credi, F. Raymo and J. F. Stoddart, *Angew. Chem., Int. Ed.*, 2000, **39**, 3348; (e) G. S. Kottas, L. I. Clarke, D. Hornek and J. Michl, *Chem. Rev.*, 2005, **105**, 1281; (f) E. R. Kay, D. A. Leigh and Z. Zerbetto, *Angew. Chem., Int. Ed.*, 2007, **46**, 72.
- (a) Z. Dominguez, H. Dang, M. J. Strouse and M. A. Garcia-Garibay, *J. Am. Chem. Soc.*, 2002, **124**, 2398; (b) C. E. Godinez, G. Zepeda and M. A. Garcia-Garibay, *J. Am. Chem. Soc.*, 2002, **124**, 4701; (c) Z. Dominguez, H. Dang, M. J. Strouse and M. A. Garcia-Garibay, *J. Am. Chem. Soc.*, 2002, **124**, 7719; (d) Z. Dominguez, T. V. Khuong, H. Dang, C. N. Sanrame, J. E. Nuñez and M. A. Garcia-Garibay, *J. Am. Chem. Soc.*, 2003, **125**, 8827; (e) C. E. Godinez, G. Zepeda, C. J. Mortko, H. Dang and M. A. Garcia-Garibay, *J. Org. Chem.*, 2004, **69**, 1652; (f) T. V. Khuong, G. Zepeda, R. Ruiz, S. I. Khan and M. A. Garcia-Garibay, *Cryst. Growth Des.*, 2004, **4**, 15; (g) S. D. Karlen, R. Ortiz, O. L. Chapman and M. A. Garcia-Garibay, *J. Am. Chem. Soc.*, 2005, **127**, 6554; (h) S. D. Karlen and M. A. Garcia-Garibay, *Chem. Commun.*, 2005, 189; (i) R. D. Horansky, L. I. Clarke, J. C. Price, T. V. Khuong, P. D. Jarowski and M. A. Garcia-Garibay, *Phys. Rev. B: Condens. Matter Mater. Phys.*, 2005, **72**, 014302; (j) S. D. Karlen, S. I. Khan and M. A. Garcia-Garibay, *Cryst. Growth Des.*, 2005, **5**, 53; (k) R. D. Horansky, L. I. Clarke, E. B. Winston, J. C. Price, S. D.

- Karlen, P. D. Jarowski, R. Santillan and M. A. Garcia-Garibay, *Phys. Rev. B: Condens. Matter Mater. Phys.*, 2006, **74**, 054306; (l) S. D. Karlen, C. E. Godinez and M. A. Garcia-Garibay, *Org. Lett.*, 2006, **8**, 3417; (m) M. A. Garcia-Garibay, *Proc. Natl. Acad. Sci. U. S. A.*, 2005, **102**, 10771; (n) T. V. Khuong, J. E. Nuñez, C. E. Godinez and M. A. Garcia-Garibay, *Acc. Chem. Res.*, 2006, **39**, 413; (o) P. D. Jarowski, K. N. Houk and M. A. Garcia-Garibay, *J. Am. Chem. Soc.*, 2007, **129**, 3110; (p) T. V. Khuong, H. Dang, P. D. Jarowski, E. F. Maverick and M. A. Garcia-Garibay, *J. Am. Chem. Soc.*, 2007, **129**, 839.
- 11 (a) T. Shima, F. Hampel and J. A. Gladysz, *Angew. Chem., Int. Ed.*, 2004, **43**, 5337; (b) L. Wang, T. Shima, F. Hampel and J. A. Gladysz, *Chem. Commun.*, 2006, 4075; (c) K. Skopec, M. C. Hershberger and J. A. Gladysz, *Coord. Chem. Rev.*, 2007, **251**, 1723; (d) G. D. Hess, F. Hampel and J. A. Gladysz, *Organometallics*, 2007, **26**, 5129; (e) W. Setaka, S. Ohmizu, C. Kabuto and M. Kira, *Chem. Lett.*, 2007, **36**, 1076.
- 12 (a) L. I. Clarke, D. Horinek, G. S. Kottas, N. Varaksa, T. F. Magnera, T. P. Hinderer, R. D. Horansky, J. Michl and J. C. Price, *Nanotechnology*, 2002, **13**, 533; (b) S. How, T. Sagara, D. Xu, T. R. Kelly and E. Ganz, *Nanotechnology*, 2003, **14**, 566; (c) J. R. Gardinier, P. J. Pellechia and M. D. Smith, *J. Am. Chem. Soc.*, 2005, **127**, 12448; (d) S. Horike, R. Matsuda, D. Tanaka, S. Matsubara, M. Mizuno, K. Endo and S. Kitagawa, *Angew. Chem., Int. Ed.*, 2006, **45**, 7226; (e) D. Horinek and J. Michl, *Proc. Natl. Acad. Sci. U. S. A.*, 2005, **102**, 14175.
- 13 (a) N. Takamatsu, T. Akutagawa, T. Hasegawa, T. Nakamura, T. Inabe, T. Fujita and K. Awaga, *Inorg. Chem.*, 2000, **39**, 870; (b) T. Akutagawa, S. Nishihara, N. Takamatsu, T. Hasegawa, T. Nakamura and T. Inabe, *J. Phys. Chem. B*, 2000, **104**, 5871; (c) T. Akutagawa, N. Takamatsu, K. Shitagami, T. Hasegawa, T. Nakamura and T. Inabe, *J. Mater. Chem.*, 2001, **11**, 2118; (d) T. Akutagawa, A. Hashimoto, S. Nishihara, T. Hasegawa and T. Nakamura, *J. Supramol. Chem.*, 2002, **2**, 175; (e) T. Akutagawa, A. Hashimoto, S. Nishihara, T. Hasegawa and T. Nakamura, *J. Phys. Chem. B*, 2003, **107**, 66; (f) S. Nishihara, T. Akutagawa, T. Hasegawa and T. Nakamura, *Inorg. Chem.*, 2003, **42**, 2480; (g) T. Akutagawa, K. Matsuura, S. Nishihara, S. Noro and T. Nakamura, *Eur. J. Inorg. Chem.*, 2005, 3271; (h) T. Akutagawa, K. Matsuura, A. Hashimoto and T. Nakamura, *Inorg. Chem.*, 2005, **44**, 4454; (i) S. Nishihara, T. Akutagawa, T. Hasegawa and T. Nakamura, *Chem. Commun.*, 2002, 408.
- 14 T. Akutagawa, H. Koshinaka, D. Sato, S. Takeda, S. Noro, H. Takahashi, R. Kumai, Y. Tokura and T. Nakamura, *Nat. Mater.*, 2009, **8**, 342.
- 15 (a) T. Akutagawa, K. Shitagami, S. Nishihara, S. Takeda, T. Hasegawa, T. Nakamura, Y. Hosokoshi, K. Inoue, S. Ikeuchi, Y. Miyazaki and K. Saito, *J. Am. Chem. Soc.*, 2005, **127**, 4397; (b) S. Ikeuchi, Y. Miyazaki, S. Takeda, T. Akutagawa, S. Nishihara, T. Nakamura and K. Saito, *J. Chem. Phys.*, 2005, **123**, 044514; (c) D. Sato, T. Akutagawa, S. Takeda, S. Noro and T. Nakamura, *Inorg. Chem.*, 2007, **46**, 363; (d) S. Nishihara, T. Akutagawa, D. Sato, S. Takeda, S. Noro and T. Nakamura, *Chem.–Asian J.*, 2007, **2**, 1083; (e) T. Akutagawa, D. Sato, H. Koshinaka, M. Aonuma, S. Noro, S. Takeda and T. Nakamura, *Inorg. Chem.*, 2008, **47**, 5951; (f) T. Akutagawa and T. Nakamura, *Dalton Trans.*, 2008, 6335; (g) T. Akutagawa, H. Koshinaka, Q. Ye, S. Noro, J. Kawamata, H. Yamaki and T. Nakamura, *Chem.–Asian J.*, 2010, **5**, 520; (h) T. Akutagawa, D. Sato, Q. Ye, S. Noro and T. Nakamura, *Dalton Trans.*, 2010, **39**, 2191.
- 16 (a) G. A. Jeffrey, *An Introduction to Hydrogen Bonding*, D. G. Truhlar ed., Oxford University Press, NY, 1997; (b) G. C. Pimentel and A. L. McClellan, *The Hydrogen Bond*, Freeman, San Francisco, 1960; (c) W. C. Hamilton and J. A. Ibers, *Hydrogen Bonding in Solids*, R. Breslow and M. Karplus ed., Benjamin Inc, NY, 1968.
- 17 T. Mori, A. Kobayashi, Y. Sasaki, H. Kobayashi, G. Saito and H. Inokuchi, *Bull. Chem. Soc. Jpn.*, 1984, **57**, 627.
- 18 J. C. Scott, *Semiconductor and Semimetals. Highly Conducting Quasi-One-Dimensional Organic Crystals*, E. Conwell, ed., Academic Press, NY, 1988, p. 385.
- 19 M. J. Frisch *et al.*, *GAUSSIAN R03W*, Gaussian, Inc., Pittsburgh, PA, 2003.
- 20 (a) E. Weber, J. L. Toner, I. Goldberg, F. Vögtle, D. A. Laidler, J. F. Stoddart, R. A. Bartsch and C. L. Liotta, *Crown ethers and analogs*, S. Patai, Z. Rappoport ed., John Wiley & Sons, NY, 1989; (b) G. W. Gokel, *Crown Ethers & Cryptands*, J. F. Stoddart ed., RSC, Cambridge, 1994; (c) O. Nagao, A. Kobayashi and Y. Sasaki, *Bull. Chem. Soc. Jpn.*, 1978, **51**, 790; (d) G. W. Buchanan, R. A. Kirby, J. A. Ripmeester and C. I. Ratcliffe, *Tetrahedron Lett.*, 1987, **28**, 4783; (e) C. I. Ratcliffe, J. A. Ripmeester, G. W. Buchanan and J. M. Denike, *J. Am. Chem. Soc.*, 1992, **114**, 3294.
- 21 K. C. Kao, *Dielectric Phenomena in Solids*, Elsevier, Amsterdam, 2004.
- 22 R. L. Carlin, *Magnetochemistry*, Springer-Verlag, Heidelberg, 1986.
- 23 (a) M. Troyer, H. Tsunetsugu and D. Würtz, *Phys. Rev. B: Condens. Matter*, 1994, **50**, 13515; (b) T. M. Rice, S. Gopalan and M. Sigrist, *Europhys. Lett.*, 1993, **23**, 445.
- 24 G. Steimecke, H. J. Sieler, R. Krimse and E. Hoyer, *Phosphorus Sulfur Relat. Elem.*, 1978, **7**, 49.
- 25 *Crystal Structure: Single crystal structure analysis software*. Ver. 3.6.2004. Rigaku Corporation and Molecular Structure Corporation; G. M. Sheldrick, *SHELX97 Programs for Crystal Structure Analysis*, Universität Göttingen, Göttingen, Germany, 1998.